Asian Journal of Atmospheric Environment
Vol. 2-2, pp.81-89, December 2008

Effects of Strong Wind and Ozone on Localized Tree Decline in the Tanzawa Mountains of Japan

Hitoshi Suto*, Yasuo Hattori, Nobukazu Tanaka and Yoshihisa Kohno

Central Research Institute of Electric Power Industry, 1646 Abiko, Abiko City, Chiba 270-1194, Japan

*Corresponding author. Tel: +81-4-7182-1181, E-mail: suto@criepi.denken.or.jp

ABSTRACT

The numerical simulation of wind and ozone (O_3) transport in mountainous regions was performed with a computational fluid dynamics technique. A dry deposition model for O_3 was designed to estimate O_3 deposition in complex terrain, and the qualitative validity of the predicted O_3 concentration field was confirmed by comparison with observed data collected with passive samplers. The simulation revealed that wind velocity increases around ridge lines and peaks of mountains. The areas with strong wind corresponded well with the sites of tree decline at high altitudes, suggesting that it is an important factor in the localization of tree/forest decline. On the other hand, there is no direct relationship between forest decline and O_3 concentration. The O_3 concentration, however, tends to increase as wind velocity becomes higher, thus the O_3 concentration itself may be a potential secondary factor in the localized decline phenomena. While the diffusion flux of O_3 is not related to localized tree decline, the pattern of advection flux is related to those of high wind velocity and localized tree decline. These results suggest that strong wind with large advection flux of O_3 may play a key role in the promotion of tree/forest decline at high mountain ridges and peaks.

Key words: Tree decline, Strong wind, Ozone, Deposition model, Computational fluid dynamics

1. INTRODUCTION

The development and distribution of tree/forest decline have been associated with multiple stress factors, such as air pollutants and natural stress factors (Kohno, 2004; UN/ECE and EC, 1999; Kohno *et al.*, 1998). For instance, recent air-quality monitoring data and an open-top chamber O_3 exposure study in beech seedlings suggested that the effects of O_3 may be associated with the tree/forest declines (Takeda and Aihara, 2005; Aso and Nakashima, 2004), while most of the tree/forest decline in remote and high mountains is confined to specific areas and may possibly be linked with meteorological factors (Koshiji *et al.*, 1996). In many cases, high mountain sites record higher O_3 concentration and significant wind speed than those at foothill sites, thus these two factors may possibly have significant empirical effect, singly and/or in combination, on tree/forest decline. There are many models for evaluating the long-distance transport and deposition of air pollutants (see, for example, Byun and Ching, 1999; Draxler and Hess, 1998). However, they are usually based on meteorological models with simple non-hydrostatic approximations occasionally optimized for coarse grid resolution, and thus may not have sufficient accuracy for the evaluation of complex terrain such as mountainous areas.

In this research, a dry deposition model combined with the computational fluid dynamics (CFD) technique is designed for evaluating O_3 deposition on complex terrains and is verified by comparison with observed data collected with passive O_3 samplers. Spatial distributions of predicted wind and O_3 are compared with the locations of ascertained sites of tree/forest decline to discuss their individual and combined effects on the declining phenomena.

2. METHOD

2.1 Computational Region

The Tanzawa Mountains of Japan was chosen for the computational region (Fig. 1(a)), because here, localized tree/forest decline is observed and O_3 concentrations are relatively high depending on elevation. In the Tanzawa Mountains located in the western part of Kanagawa Prefecture, declined Japanese beech trees (*Fagus crenata*) are conspicuous in the southern to southwestern slopes along the ridges and at high peaks. Recent study (Takeda and Aihara, 2005; Aso and Nakashima, 2004) suggested that O_3 may be associated with those declines as previously described.

To take the influence of the wind direction into account and to prepare time-averaged distribution maps

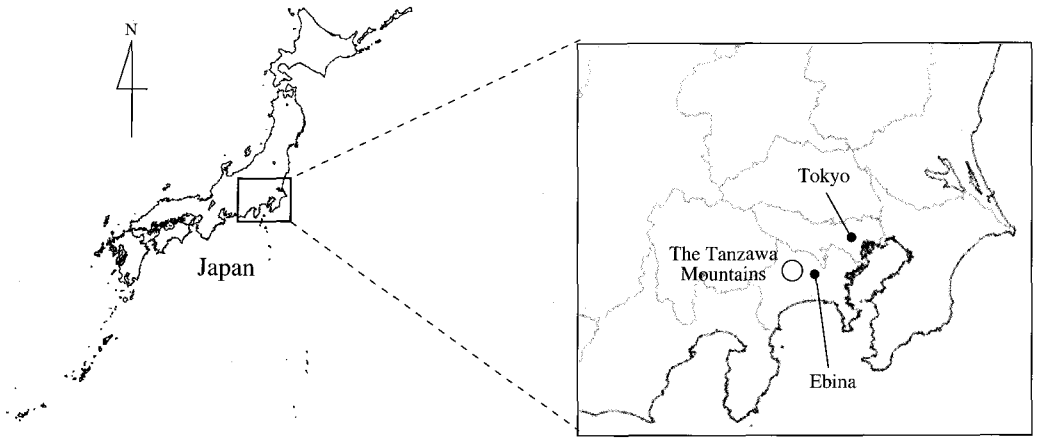

(a) Location of computational region

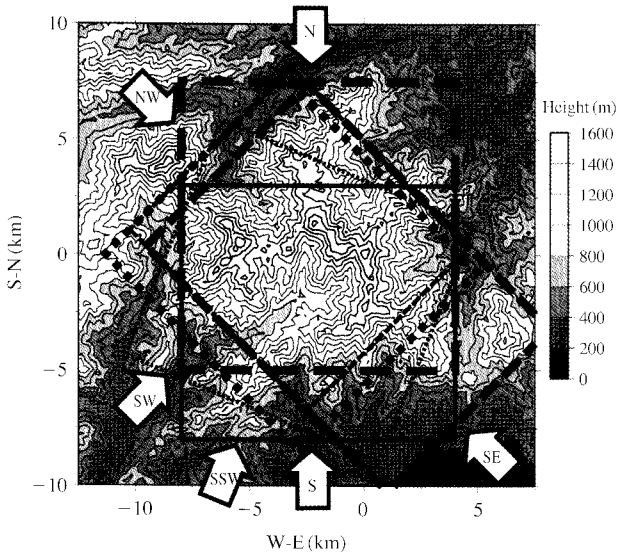

(b) Computational domain

Fig. 1. Computational region.

of wind and O_3 concentration, six main wind directions are chosen using data (Ebina, 2002-2004) obtained by AMeDAS (Automated Meteorological Data Acquisition System) from the Japan Meteorological Agency (Fig. 1(a)). Rectangular computational domains set for each main wind direction are shown in Fig. 1(b).

2.2 Computational Method

In this study, we assume atmospheric conditions of incompressible dry air under neutral stratification. Wind and O_3 transport above a forest canopy layer are simulated, and those in a canopy layer are not directly solved since they are modeled under the ground boundary condition. In order to accurately predict local wind in complex terrains, the continuity, Navier-Stokes and concentration transport equations described in boundary-fitted coordinates are used as basic equations:

$$\frac{\partial U_c^k}{\partial \xi^k}=0, \tag{1}$$

$$\frac{\partial U_i}{\partial t}+\frac{U_c^k}{J}\frac{\partial U_i}{\partial \xi^k}=-\frac{1}{\rho}\frac{\partial \xi^k}{\partial x_i}\frac{\partial P}{\partial \xi^k}+\frac{1}{J}\frac{\partial}{\partial \xi^k}\left(\nu_t h_{kl}\frac{\partial U_i}{\partial \xi^l}\right), \tag{2}$$

$$\frac{\partial C}{\partial t}+\frac{U_c^k}{J}\frac{\partial C}{\partial \xi^k}=\frac{1}{J}\frac{\partial}{\partial \xi^k}\left(D_t h_{kl}\frac{\partial C}{\partial \xi^l}\right), \tag{3}$$

Table 1. Computational condition.

Computational region	Main wind direction	Inlet concentration, C_0/C_a	Grid points Nx, Ny, Nz (max)	Δx [m]	Δy [m]	Δz [m] (min, max)
Tanzawa Mountains	SE, S, SSW, SW, NW, N	0.8	301 × 241 × 30	50	50	10, 2380

where

x_i =(x, y, z) : Cartesian coordinates (x : main wind direction, y : horizontal direction perpendicular to x, z : vertical direction) [m],
ξ^k =(ξ, η, ζ) : boundary-fitted coordinates [m],
U_i =(U, V, W) : velocity components in (x, y, z) direction [m/s],
U_c^k=(U_c, V_c, W_c) : contravariant velocity components in (ξ, η, ζ) direction [m/s],
C : O_3 concentration [kg/m^3],
t : time [s],
ρ : density of atmosphere [kg/m^3],
$h_{kl}=\frac{\partial \xi^k}{\partial x_m}\frac{\partial \xi^l}{\partial x_m}$: fundamental tensor,
J : Jacobian,
ν_t : eddy kinetic viscosity [m^2/s],
D_t : eddy diffusivity of ozone [m^2/s].

In this simulation, the standard k-ε model is used in order to deduce the eddy kinetic viscosity, and the turbulent Schmidt number is set to 1. Photochemical reactions are omitted since the time scale of the reaction is larger than that of wind flow, and advection must be dominant in the narrow regions of about 10 km × 10 km considered here. The third-order upwind finite difference is applied to the advection terms and the second-order central finite difference is applied to the diffusion terms for the discretization of basic equations. The Crank-Nicholson method is used for time development. On the inlet boundary, the logarithmic profiles are given to both the velocity and the concentration on the basis of the analogy between momentum and mass transfer, and the concentration at the ground level is set at 80 percent of the upper air concentration by referring to observation data (Aso and Nakashima, 2004). The convection condition is applied at the outlet boundary, and the free-slip condition of velocity and the zero-flux condition of concentration are imposed on the upper and side boundaries, respectively. On the ground boundary, we apply the logarithmic law of velocity and the equilibrium condition of the concentration diffusion flux and the deposition flux above a canopy layer,

$$D_t\frac{\partial C}{\partial z}=V_dC, \tag{4}$$

where V_d is deposition velocity. To take account of the wind velocity dependence of V_d, it is divided into the aerodynamic resistance r_a, the quasi-laminar layer resistance r_b and the surface resistance r_c. Then, r_a and r_b are directly calculated from the wind simulation and r_c is set to be 200 s/m on the basis of existing literatures (Matsuda *et al.*, 2005). This ground boundary condition for O_3 deposition is fundamentally valid for a flat terrain, and the effect of a complex terrain on deposition is elucidated through eddy diffusivity D_t and concentration C, which are spatially varied by local wind. The validity of this model is discussed in section 3.1.

Computational conditions are shown in Table 1. Subscripts '0' and 'a' in the table indicate the ground surface (a ground height of 0 m) and the height of the upper wind level (350 m), respectively. Assuming the background O_3 originates from the stratosphere or distant urban centers, the inlet O_3 concentration exhibits a logarithmic profile which has positive gradients in the vertical direction. Grid points are allocated at even intervals in the horizontal (x, y) plane and densely near the ground in the vertical direction.

3. RESULTS AND DISCUSSION

3.1 Evaluation of Deposition Model

The validity of this wind simulation has already been confirmed, by comparisons of the simulation results with the results of wind tunnel experiments and wind observations, to show high performance (Hattori *et al.*, 2003), while the validity of the dry deposition model and the computational method for O_3 transport have not yet been examined. Thus, the O_3 concentration obtained by the simulation was compared with that observed in the Tanzawa Mountains (Aso and Nakashima, 2004).

The observational measurement by Aso and Nakashima (2004) was conducted using an Ogawa passive sampling system from May to September in 2004. The ground height of diffusion samplers was approximately 1.5 m. The exposure time was two weeks. The trapping part (filter paper) of the samplers was impregnated with 50 μg of 1 percent $NaNO_2$ solution. While the samplers were exposed, $NaNO_3$ was formed in proportion to O_3 concentration by the reaction '$NaNO_2$

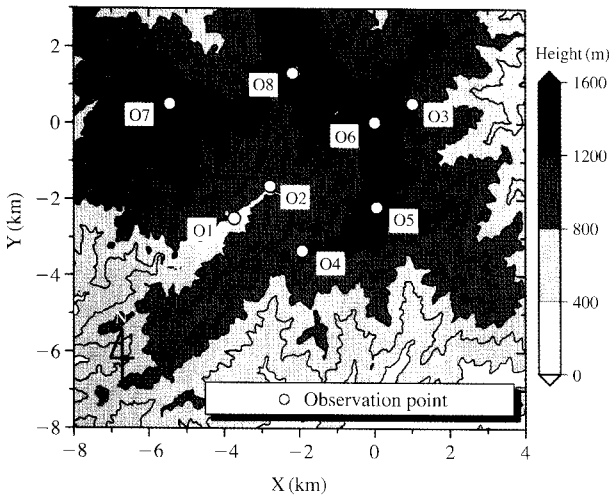

Fig. 2. Location of observation points in Tanzawa Mountains.

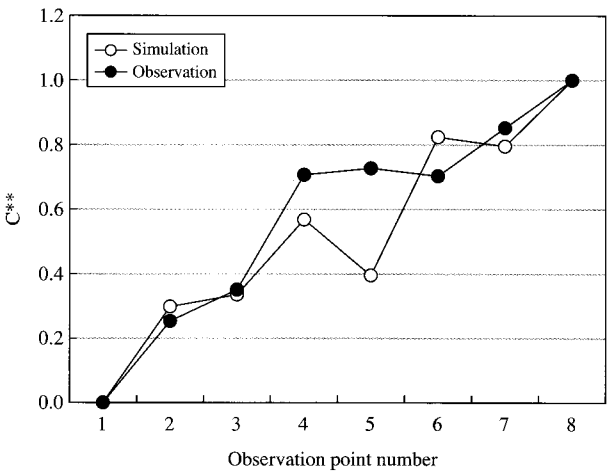

Fig. 3. Comparison of O_3 concentration between passive sampling data and simulation in Tanzawa Mountains. Vertical scale: O_3 concentration normalized by the concentration at the point O1 and the point O8. Locations of the observation points are shown in Fig. 2.

$+O_3 \rightarrow NaNO_3+O_2$'. After they were removed and NO_3^- was analyzed using ion chromatography, O_3 concentration was deduced using the correlation function between O_3 concentration and the rates of NO_3^- conversion.

Since the observation data were time-averaged concentrations in the period, corresponding averaged values were calculated from the numerical results of the six main wind directions by the time-averaging method described in section 3.2. The locations of eight observation points (O1-O8) are shown in Fig. 2, and numerical results and observation results at those eight points are compared in Fig. 3. The horizontal axis in Fig. 3 is the observation point number arranged in the order of altitude, and the vertical axis is the O_3 concentration, which is normalized by the concentration at point O1 (an altitude of 175 m) and point O8 (an altitude of 1,672 m) in the figure ($C^{**}=(C-C_{O1})/(C_{O8}-C_{O1})$) to verify the relative magnitude between the points. The numerical results agree well with the observation results on the points O1-O4 and O6-O8, while the difference between the two results is comparatively large at point O5. This might be caused by an inappropriate inlet boundary condition of O_3 concentration, because point O5 is near the inlet boundary in the case of a S or SSW wind direction with a high occurrence frequency. Although the validation of the computational method for O_3 transport is insufficient and there is room for improvement of the model and inlet boundary conditions, the results suggested that this simulation could predict the qualitative tendency of the O_3 concentration field. In the following sections, we proceed with the discussion on the relationship between wind, O_3 and localized tree decline.

3.2 Spatial Distributions of Wind and O_3

To investigate the influence of wind and O_3 on trees, attention is paid mainly to wind and O_3 concentration at a ground height of 10 m, which corresponds to the height of trees. Figs. 4, 5 show wind velocity, turbulent energy and O_3 concentration for each of S and N main wind directions with high occurrence frequency, respectively. The presentation of the results of the other main wind directions are omitted, since similar tendencies were found in the examination, as described below. The contours in the figures are normalized by the values at the inlet boundary. Small arrows and black and white lines in these figures show local wind directions, altitude contours and the rough locations of distinctive U-shaped ridges, respectively. Wind velocity increases on the upwind slopes of the U-shaped ridge and its branch lines, while wind weakens on the downwind slopes and valleys. As observed in Fig. 6 showing the amplitude of wind velocity in a vertical section (y=2 km in Fig. 4(a)), such wind variations near the ground are closely related to the variation in the thickness of the atmospheric boundary layer caused by the ground slope and to the separation of high-velocity flow behind mountains. Moreover, turbulent energy increases in the areas with high wind velocity, supporting the fact that the increase in wind velocity on the upwind slopes is caused by enhanced atmospheric shear, which is directly related to turbulent intensity.

The O_3 concentration also show an increasing tendency on the upwind slopes of ridges at high altitude,

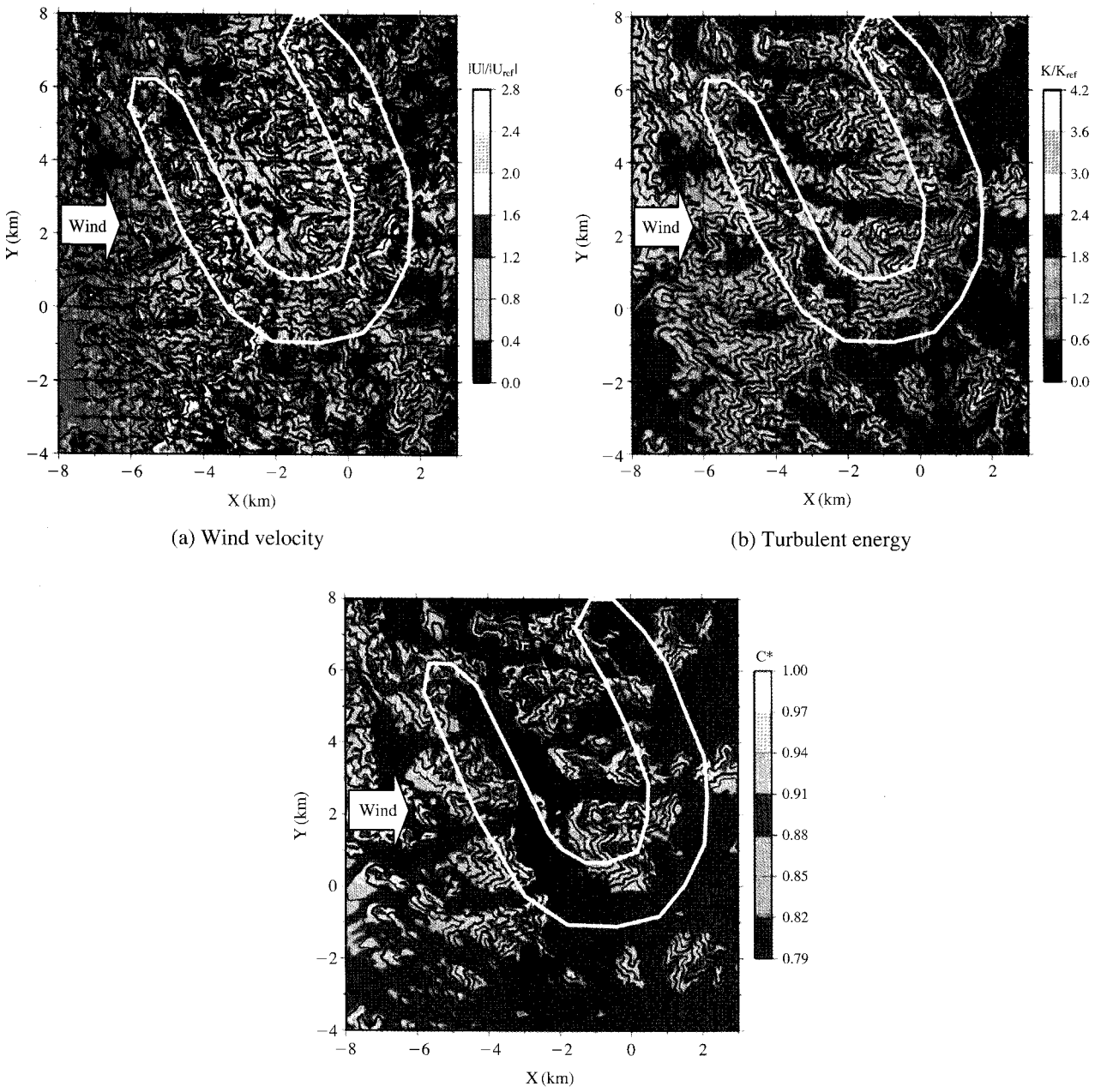

(a) Wind velocity

(b) Turbulent energy

(c) O_3 concentration

Fig. 4. Distribution at the ground height of 10 m (S main wind direction).

since the O_3 transport from the upper air to the ground is here promoted by the increase in turbulence (Fig. 7). As a result, the distribution of O_3 concentration is essentially similar to those of wind velocity and turbulent energy, though the spatial variation of the concentration is smaller than that of wind field.

Among the results in the cases of S and N main wind directions, the locations with high wind velocity and high O_3 concentration are naturally different. However, they take maximum values near ridge lines in both cases, suggesting that such areas should be potentially affected by strong wind and high O_3 concentration.

3.3 Advection Flux and Diffusion Flux

Localized tree/forest decline phenomena may be related to the finding that wind velocity and O_3 concentration vary near the ground surface in the complex terrains, as described in the previous section. In this

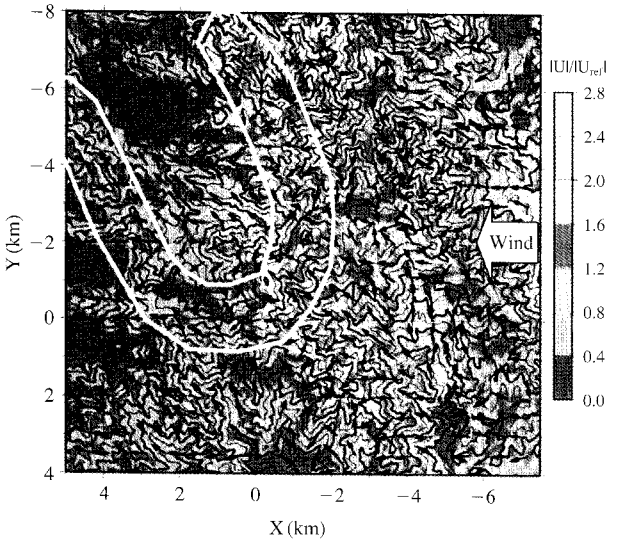

(a) Wind velocity

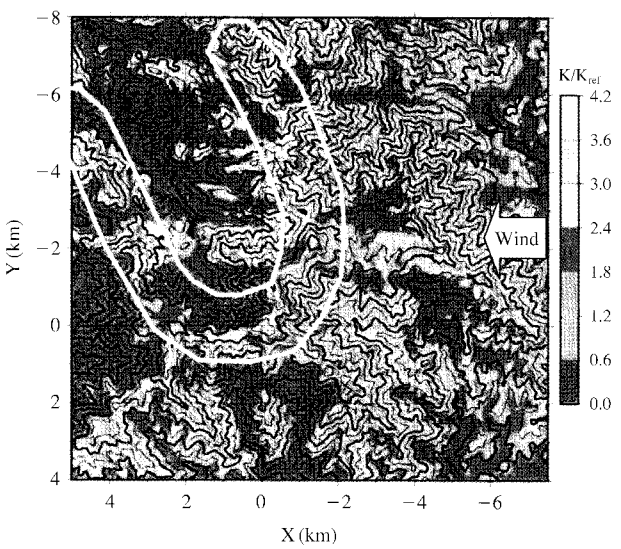

(b) Turbulent energy

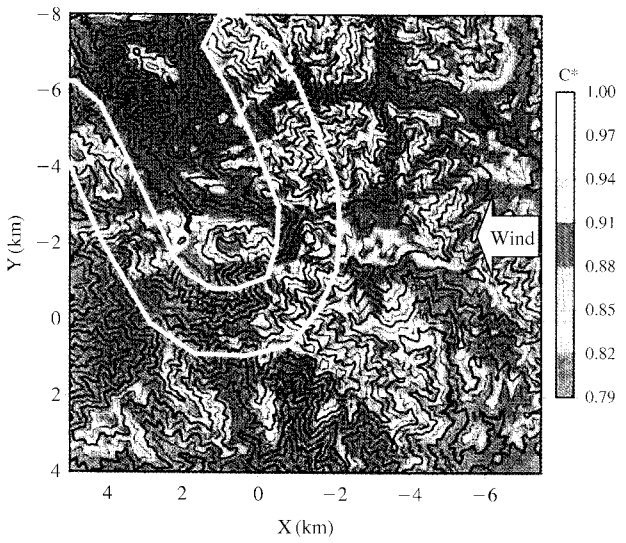

(c) O_3 concentration

Fig. 5. Distribution at the ground height of 10 m (N main wind direction).

section, attention is paid to the advection flux $F_C=U_pC$, which shows the amount of a substance transported parallel to the ground surface, and the diffusion flux $F_D=-D_t\partial C/\partial n$, which is usually used for the evaluation of the amount of deposition, where 'p' and 'n' denote the ground-parallel and ground-vertical components of wind velocity. The correlation component of velocity fluctuation and concentration fluctuation in F_C is omitted since it is comparatively small.

Figs. 8 and 9 show the distributions of normalized advection flux and diffusion flux near the ground in the case of S main wind direction. The contour of advection flux is highly similar to that of wind velocity. This is caused by the larger variation of wind velocity than that of O_3 concentration, showing that the wind field substantially dominates the advective transport of O_3. On the other hand, the spatial variation of diffusion flux is quite small.

3.4 Time-averaged Distributions and Localized Tree Decline

Since trees/forests should declined owing to the

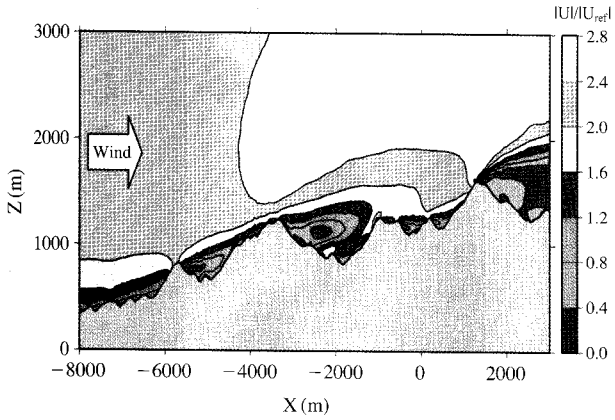

Fig. 6. Vertical distribution of wind velocity at Y=2 km (S main wind direction).

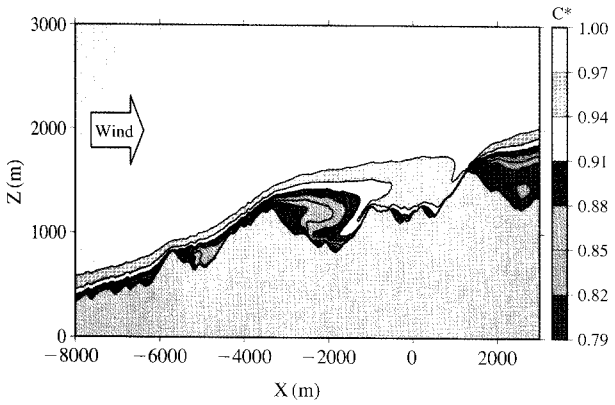

Fig. 7. Vertical distribution of O_3 concentration at Y=2 km (S main wind direction).

cumulative influence of strong wind and O_3 for example, time-averaged values of wind velocity, concentration, advection flux and diffusion flux of O_3 are calculated using the following equation so as to evaluate the numerical results in cumulative time:

$$\phi_{mean}=\sum_{WD}(R_{WD}\cdot\phi^{(WD)}),\ \phi=U_H,\ C,\ F_A,\ F_D. \qquad (5)$$

Here, U_H, WD and R_{WD} are the velocity of strong wind, the direction of strong wind and the occurrence frequency of WD, respectively. 'Strong wind' is here defined as wind with higher velocity than 'mean wind velocity'+'standard deviation of fluctuating wind' in the observation data. R_{WD} is deduced from observation data. Figs. 10-13 show the time-averaged distributions of wind velocity, O_3 concentration and both the fluxes near the ground, respectively. The ellipses in these figures indicate rough locations of the ascertained tree declined areas (D1-D3) where trees visual-

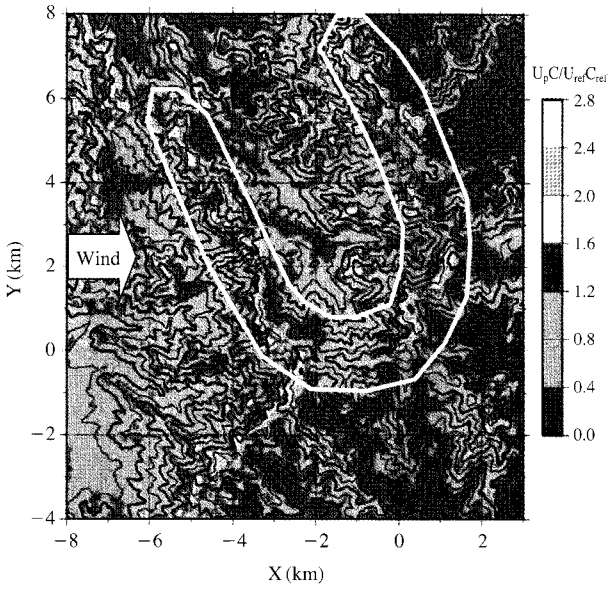

Fig. 8. Distribution of advection flux at the ground height of 14 m (S main wind direction).

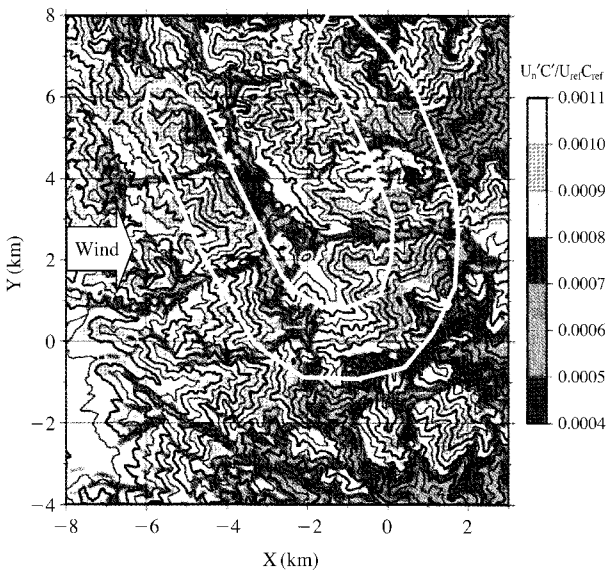

Fig. 9. Distribution of diffusion flux at the ground height of 14 m (S main wind direction).

ly recognized to be obviously dead or reduced vitality. Wind velocity and O_3 concentration vary according to the ups and downs of the ground surface and show maximum values near ridge lines and peaks of mountains. Such a variation near the ground surface has a close connection with the variation of the thickness of the velocity boundary layer and the flow separation behind mountains, as mentioned in the section 3.2.

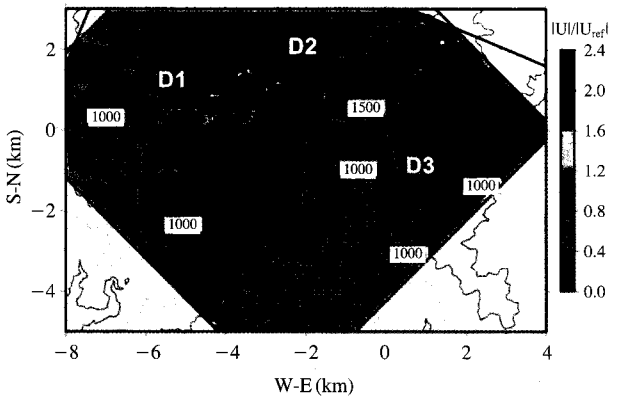

Fig. 10. Time-averaged wind velocity.

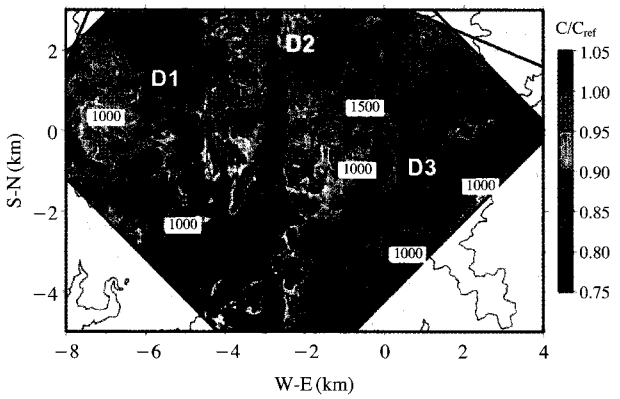

Fig. 11. Time-averaged O_3 concentration.

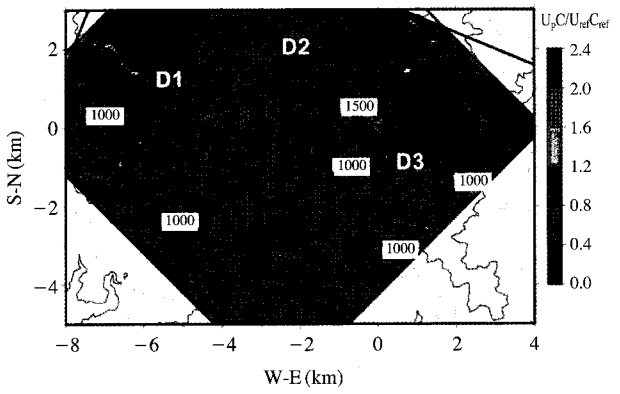

Fig. 12. Time-averaged O_3 advection flux.

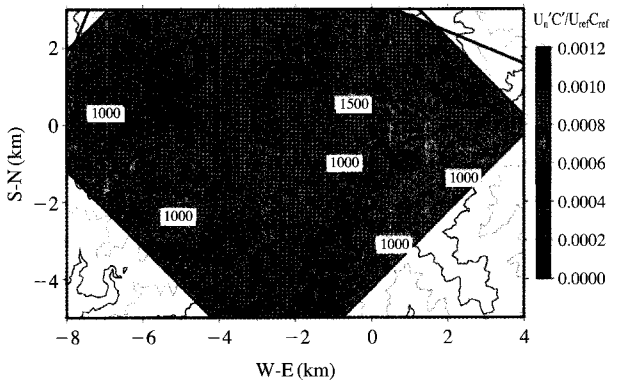

Fig. 13. Time-averaged O_3 diffusion flux.

The ascertained tree decline areas correspond well with high-wind-velocity areas near ridge line and peaks, suggesting that the localization of tree/forest decline is strongly influenced by local wind properties, which probably also are related to the evaporation of moisture from trees. On the other hand, the spatial variation of O_3 concentration is much smaller than that of wind velocity, and no clear relationship between the distribution of O_3 concentration and tree decline is found. The similarity in the velocity field and O_3 concentration field, however, suggests that the concentration itself has the possibility of being a secondary factor in the localized decline phenomena in a region with high O_3 concentration.

Advection flux, which is greatly affected by wind, shows good correspondence with the tree decline areas, while the distribution of diffusion flux is nearly constant and does not show a clear correspondence. When considering the impact of ozone on trees/forest, the advection flux should be regarded as a combined influence of wind and O_3, and it seems to have a closer connection with the localized tree/forest decline than the O_3 concentration itself. However, it is not valid if wind and ozone have compound effects (as on the flux), and further ecophysiological observations, particularly of factors such as stomatal conductance, evapotranspiration, and water conditions, are required to evaluate these numerical results.

4. CONCLUSIONS

The numerical simulation of wind and O_3 transport in mountains was conducted by the CFD technique. By comparing the location of tree decline areas with wind, O_3 concentration, O_3 advection flux and O_3 diffusion flux, their influence on the decline was examined. Conclusions are summarized as below.

(1) The numerical data, compared with observed data, successfully predict the qualitative tendency of the O_3 concentration field. On the other hand, further validation of the computational method is needed for the quantitive evaluation of the O_3 concentration.

(2) Wind velocity near the ground increases around ridge lines or peaks of mountains. The areas of strong wind correspond well with the tree decline areas, suggesting wind to be one of the important factors in localized tree decline.

(3) There is no direct relationship between forest decline and O_3 concentration. However, the concentration tends to increase as wind velocity becomes high, thus the concentration itself may be a secondary factor in the localized decline phenomena in the region with high O_3 concentration.

(4) While the diffusion flux was not related to localized tree decline, the pattern of advection flux of O_3 was related to those of high wind velocity and localized tree decline. Strong wind with a large advection flux of O_3 may play a key role in the promotion of tree/forest decline at the high mountain ridges and peaks.

ACKNOWLEDGEMENTS

This research was supported by the Global Environment Research Fund from the Ministry of the Environment of Japan. We are indebted to Kanagawa Environmental Research Center and Kanagawa Natural Environment Conservation Center (Kanagawa Prefecture, Japan) for providing valuable observation data. We are grateful to Prof. Kazuhide Matsuda of Meisei University, Dr. Snin-ichi Fujita and Dr. Hiroshi Hayami of Central Research Institute of Electric Power Industry for their helpful advice. We also wish to express our gratitude to Mr. Kiyoshi Kanzaki of Denryoku Computing Center, Ltd. for his help in performing the simulation.

REFERENCES

Aso T. and N. Nakashima (2004) Study on the distribution of ozone concentration at Hinokiboramaru and the decline of Japanese beech trees, Bulletin of Kanagawa Environmental Research Center, 27, 113-115. (translated from Japanese)

Byun D.W. and J.K.S. Ching (1999) Science Algorithms of the EPA models-3 Community Multiscale Air Quality (CMAQ) modeling system, U.S. Environmental Protection Agency, EPA/600/R-99/030.

Draxler R.R. and G.D. Hess (1998) An overview of the HYSPLIT_4 modelling system for trajectories, dispersion, and deposition. Australian Meteorological Magazine, 47, 295-308.

Hattori Y., S. Okuda, T. Ishikawa, and H. Kato (2003) Denchuken review No. 48, Central research institute of electric power industry, pp. 39-43. (in Japanese)

Kohno Y. (2004) Current status of forest decline and related monitoring programs (I) Europe and northern America. Journal of Japan Society for Atmospheric Environment, 39(1), A1-A8. (in Japanese)

Kohno Y., H. Matsumura, and T. Kobayashi (1998) Differential sensitivity of trees to simulated acid rain or ozone in combination with sulfur dioxide, Acid deposition and ecosystem sensitivity in East Asia, Nova Science Publishers, Inc., pp. 143-188.

Koshiji M., K. Suzuki, and K. Suga (1996) Investigation of forest decline in the Tanzawa Mountain (1) Distribution of decline of *Fagus crenata, Abies firma* and other tree species. Bulletin of Kanagawa Prefecture Forest Research Institute, 22, 7-18. (in Japanese)

Matsuda K., I. Watanabe, V. Wingpud, P. Theramongkol, P. Khummongkol, S. Wangwongwatana, and T. Totsuka (2005) Ozone dry deposition above a tropical forest in the dry season in northern Thailand. Atmospheric Environment, 39, 2571-2577.

Takeda M. and K. Aihara (2005) Effects of environmental ozone in the Tanzawa mountains on young Japanese beech trees, Bulletin of Kanagawa Environmental Research Center, 28, 88-89. (translated from Japanese)

UN/ECE and EC (1999) Forest condition in Europe, 1999 Executive Report, ISSN: 1020-587X.

(Received 5 October 2008, accepted 11 November 2008)